VIRAL SIZE STANDARDS FROM THE CHRONIC BEE PARALYSIS VIRUS (37 NM) AND ITS SATELLITE (17 NM)

Juan Fernandez de la Mora [a] and David Wick[b]

[a] Yale University, Department of Mechanical Engineering, New Haven, CT 06520
[b] BVS, Inc., Stevensville, MT 59870

Prepared for submission to J. Aerosol Science
3/June/2020

ABSTRACT

The Chronic Bee Paralysis Virus (CBPV) can be obtained and purified from sick or dead bees, and identified by mobility measurements via electrospray charge reduction with a differential mobility analyzer (DMA). They are studied here with a high resolution DMA that reveals three peaks. The dominant one at about 37 nm is very narrow and has a weaker and broader well resolved shoulder 4.5% more mobile. This shoulder has not been previously reported and may be due to empty (genome-free) particles. We observe another sharp peak at approximately 17 nm, likely associated with the known CBPV Satellite (CBPVS). The 17 and 37 nm peaks offer size and mobility standards considerably narrower than previously reported at any size above 5 nm, with FWHM as small as 0.02). These standards should be useful to determine the resolving power of aerosol sizing instruments with greater accuracy than formerly possible.

1. INTRODUCTION

The availability of particles with narrow size distributions has been vital in the development of aerosol sizing instruments. Polystyrene latex particles with certified dimensions have been widely used to measure the size dependence of the response of various aerodynamic and other instruments whose calculation is problematic in complex flow fields. Numerous narrow size standards are commercially available at average sizes in the micron range, with standard deviations as small as 1%. Various molecular ions have been used as mobility standards that produce spectral peaks whose width is always limited by the instrument, and are therefore believed to be essentially monomobile. As an example, DMA resolving powers (the inverse of the relative full peak width at half maximum, FWHM) of 110 in mobility have been reported for a parallel plate DMA with ions of tetraheptylammonion (THA^+). This corresponds to a resolution of 220 in diameter, and a relative standard deviation σ=FWHM/[8 ln(2)]$^{1/2}$=0.46%. This measured value was close to the ideally expected one for the instrument, so the contribution to this width associated to the mobility standard itself must be much smaller than 0.46%. Molecular size standards produced by electrosprays (Fenn et al. 1989) have accordingly enabled the precise direct determination of the resolving power of DMAs, and have as a result enabled drastic improvement in their resolving power in the 1-5 nm size range.

Unfortunately, the σ value for particle standards available in the wide size range between 5 and 500 nm is considerably larger than 1%. This is the size range of large proteins and viral particles, whence the possibility of using *bionanoparticles* (You et al. 2014) as size standards has already stimulated an interesting literature. Dave's remarks here on prior use of viruses as size standards. Such studies have been based on the pioneering work of Kaufman et al. (1993, 1996) electrospraying (ES) aqueous protein solutions followed by charge reduction (ESCR) to produce

aerosols of essentially pure species with diameters from 3 nm up to at least 200 nm. The majority of the published protein studies have been carried out not in DMAs, but in drift time ion mobility spectrometers (IMS), generally connected in series to a mass spectrometer. Although some if these IMS systems have had resolving powers as high as 200 (Clemmer), measured protein mobility peaks have typically been much wider than the intrinsic instrument line-width, presumably because proteins do not have the rigid structure of small molecular ions, offering naturally a range of rapidly interconverting geometries. The situation in mobility studies based on DMAs is even less favorable than in IMS-MS studies for two reasons. First, adducts attached to the protein can be removed in IMS-MS first by energetic collisions in the vacuum system of the MS, as well as filtered out by examining the mobility distribution only of ions with a specific mass. Because neither of these cleaning procedures is applicable at atmospheric pressure, the narrowest reported protein widths observed with a DMAs are about FWHM~3% (versus about 2% in IMS-MS studies), and are typically substantially larger. We are not aware of any report on exceptions to this rule, suggesting that protein ions in the gas phase are not ideal standards for either size or mobility. Whether or not viral particles may provide size standards with narrower size distributions than proteins is presently unclear. We have recently reviewed the substantial existing virus/DMA literature (Ref 2020) where most prior studies show relatively wide peaks with FWHM >0.1. There are, however a few encouraging exceptions with FWHM values as small as 3.9% (Kallinger et al. 2013)) obtained on a special DMA developed by Reischl and colleagues. There is also one exception based on TSI's nanoDMA operated under especial conditions reporting FWHM = 4.9% (You et al. 2014). All these DMA studies have involved viral particles in relatively low charge states *z*, typically *z* =1 or 2. This prior literature suggests that even the narrowest observed widths are limited by the DMA rather than the virus particle, providing some hope that viral particles might provide excellent size standards. This point was however difficult to demonstrate with then existing DMAs, requiring improved instrumentation like the one used in the present article.

The narrowest viral mobility peaks in the literature, approaching FWHM=2%, have been obtained via IMS-MS of the Hepatitis B virus (HBV) capsid. This work differs from most DMA studies in two ways which may perhaps be non-trivial. The HBV capsid did not contain genetic material and carried several hundred elementary charges (Uetrecht et al. 2010). It is apparently not possible to extend these IMS-MS studies to the full viral particle because the associated slight mass variability of the genetic cargo combined with the high z precludes the identification of isolated mass peaks from which to infer both the mobility and the charge state. Nor can IMS-MS experiments be carried out at small *z* due to the limited mass/charge range of most mass spectrometers.

In order to obtain better lower bounds on how narrow viral mobility peaks can be, we have recently developed a DMA specially designed to cover the viral size range at high resolution. Based on the use of molecular size standards we were able to show that its resolving power exceeded 30 (Perez-Lorenzo et al. 2020), but were not able to demonstrate higher resolutions at any particle size due to the lack of size standards with narrow size distributions in the 20-100 nm range. It seemed clear that a parallel effort in improving both the viral particle standards and the DMA was essential for further progress. Consequently we have built a variant of our prior viral DMA which will be used here to characterize the first viral particles available to us in sufficient quantities to enable optimization of the sample preparation and the overall experimental system.

2. EXPERIMENTAL

Viral particle preparation. The sample was prepared at BVS Inc by the same procedure previously described. Briefly, infected bees are collected from the vicinity of the beehive. 6 g of

bees are added to 40 ml of water purified by reverse osmosis (RO), mixing them in a blender for 2 minutes. The material is then drained through a three layer cheesecloth to remove large fragments such as insect wings and legs. It is subsequently centrifuged at 20,000 relative centrifugal gravities to separate to the bottom of the vial cell fragments and other comparably large objects. The supernatant recovered is mixed with 500 ml of RO water and run past a 500 kDa hollow fiber tangential filter that removes particles smaller than about 7 nm and reduces the volume to 2 ml. This sample is then diluted 10-fold into a 10 mM aqueous solution of ammonium acetate for analysis at BVS. The samples sent to Yale were diluted (also ten-fold) in deionized water without salt addition. Both samples were also cleaned with a 0.45 μm mixed cellulose ester filter. All the samples sent to Yale were independently analyzed at BVS based on TSI's nanoDMA (model 3080) with TSI's electrospray charge reduction model 3480 and detected with TSI's condensation particle counter (CPC) 3772. BVS's spectra averaged 5 mobility scans each of 90 s at an electrospray flow rate of 40 nL/min. We should note that we have no absolute certainty of the nature of the virus in a given sample, as different beehives may suffer different infections at different times, often with closely related virions. A reasonably reliable determination was made at BVS based on the particle size measured there with TSI's commercial system. SHOW BVS spectrum here, ideally for 8445 sample. Some samples showed more than one viral peaks in comparable abundances at BVS, but when studied a few days later at Yale only one of the two peaks was clearly present, sometimes with the other seen only in trace quantities. A relatively common infection is that of the Chronic Bee Paralysis Virus (CBPV), with a mobility size of about 37 nm. This particle was robustly preserved during the shipment from BVS to Yale, and, once refrigerated, maintained high stability in deionized water for many weeks. The aqueous BVS samples were first analyzed as received and gave fairly sharp viral peaks over a slowly varying background. The background could be considerably reduced by several stages of dialysis, which also contributed to narrowing the peaks. All the high resolution spectra shown here therefore correspond to the further dialyzed samples.

DMA circuit. The instrument used at Yale will be described in detail elsewhere (Perez-Lorenzo et al. 2021). It is a variant of the viral DMA of Perez-Lorenzo et al. (2019), with a considerably wider laminarization trumpet and a larger transition radius in the section matching the conical trumpet (30^o semi-angle) to the outer cylindrical electrode. The DMA was operated in a closed circuit of sheath gas with a pump and a heat exchanger identical to those of Perez-Lorenzo et al. (2019) The flow rate Q of sheath gas was controlled through the power applied to the blower at flow rates above about ~100 lit/min, and with a throttle valve in the flow circuit at smaller flow rates. Q was measured with a mass flow meter (Ref) up to 220 sL/min. At flow rates above 220 sL/min Q was inferred from the assumption that it is strictly proportional to the voltages at which a given peak appears, with the proportionality constant determined for a given viral particle from a spectrum taken at $Q < 220$ sL/min.

Aerosol generation. A sample flow of 0.6 L/min was drawn by the detector pump from the ambient (without any drying) through a HEPA filter, and went through the bipolar ES source described by Fernandez de la Mora and Barrios (2017). The positive capillary sprayed nine parts of the originally purely aqueous viral sample from BVS with one part of 1 M aqueous ammonium acetate buffer to produce a 100 mM concentration of this salt. The negative capillary facing the positive capillary for charge reduction of the viral particles sprayed deionized (DI) water. In previous work the negative emitter electrosprayed 50-100 mM ammonium acetate in methanol. However, we find that DI water is as effective for charge reduction. The solution is not conductive

enough to produce an electrospray or sustain a discharge similar to those from a metal tip or the meniscus of a more conducting liquid. Rather, the meniscus is approximately hemispherical and emits currents easily controllable by the voltage applied to the liquid reservoir in the range from 10 to several hundred nA. These values naturally depend on the quality of the water. The negative current chosen for most of our experiments was in the vicinity of 140 nA, while that for the positive capillary ranged from 200 to 300 nA. Two concrete advantages of the present negative buffer are: (i) no need to monitor that the spray operates in the cone jet more; (ii) wide range of currents available; (iii) The quality of water is generally higher than that of methanol resulting in lesser contamination from charge reduction. The emitting tips had diameters of about 30 μm, drawn under a flame from capillaries with inner and outer diameters of 150 and 360 μm. The two capillaries were electrostatically isolated by placing a 30% transparent grounded stainless steel screen in between. The gas flow carried the charge-reduced particles from the electrospray chamber into the aerosol inlet of the DMA.

Detector. We used Kanomax's fast CPC without sheath gas and with a sample flow rate of 0.6 Lit/min. Pulses were counted over a certain dwell time *t* and are represented as counts/s by dividing the total counts detected by the dwell time.

Acquisition of mobility spectra. A home made computer program stepped through a set of equally spaced voltages and stored the response in counts/s versus the DMA voltage. A raw mobility spectrum is just a representation of one of these variables versus the other.

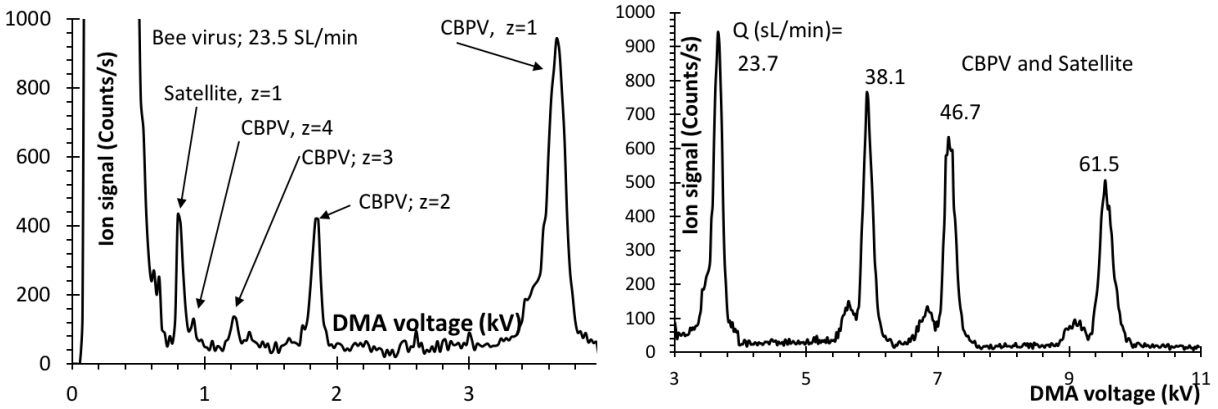

Figure 1: Mobility spectra from a bee sample. Left: full spectrum taken at a sheath gas flow rate *Q*=23.7 L/min, showing a dominant singly charged ion for the CBPV, with additional smaller peaks for charge states *z*=2, 3, 4. The most mobile peak arising at 815 V corresponds to the so called CBPV satellite. Right: Four partial spectra showing the main peak obtained at the various indicated sheath gas flow rates. The resolving power increases substantially with *Q*, resulting in almost complete separation of the shoulder at the largest flow rates.

3. RESULTS AND DISCUSSION

Figure 1 (left) shows a raw mobility spectrum taken at a sheath gas flow rate *Q*=23.7 L/min No ion signal was discernible above the background at voltages larger than those shown. A much larger signal ascribed to proteins arises at low voltages, while the background of about 30 counts/s is due to real particles present with the viral particles. The latter are concentrated over rather narrow voltage ranges and are clearly discernible from the slowly varying background. The main peak appearing at 3.66 kV corresponds to CBPV with a single charge (*z*=1), while three other smaller peaks appearing at ½, 1/3 and ¼ of that voltage correspond to the same particle in charge

states *z* of 2, 3 and 4. The CBPV peak has a shoulder at a slightly lower voltage, clearly recognizable at charge states *z*=1 and 2. This shoulder has not been previously reported and may be due to empty (genome-free) particles [Add relevant discussion on either empty capsids or other viri with a very similar size and symptoms, as well as references from Dave]. One can in addition see a substantial peak at 0.815 kV that may be ascribed to the so called satellite of CBPV (CBPVS; Ribière et al. 2010). Figure 1 right shows four spectra for the main peak obtained at different sheath gas flow rates *Q* as indicated in the Figure labels. The four different spectra appear to lay in a single curve because the data were taken by stepping the voltage at fixed *Q* until the peak was swept, pausing the voltage scan and stabilizing the flow rate at a larger value, and resuming the voltage scan at that new fixed *Q*. The resolving power increases substantially with *Q*, resulting in a progressive conversion of the shoulder into an isolated peak. In an additional series of measurements at different flow rates we have captured this peak at a voltage of 10.46 kV (*Q*=67.3 sL/min), quite near the maximum voltage provided by our power supply. The peaks obtained at the highest resolutions exhibit a slightly asymmetric shape, with a rise on its left side clearly sharper than its decay on the right side. This feature may be due to either the presence of another peak of slightly larger size, or (more likely) to attachment of involatile solution contaminants to some of the viral particles. In this later hypothesis the right tails would depend on the quality of the spray, increasing with the initial volume of the spray drops and the concentration of contaminants. A strong effect of the quality of the spray on peak width is indeed observed, and is moderated by operating strictly in the steady cone-jet mode at positive spray currents below 300 nA. The right tail shown by the CPBV peak also tends to increase with time after adding ammonium acetate to the aqueous viral solution to bring it to 90 mM for electrospraying. The spectra of Figure 1 are taken only hours after addition of the salt. Figure 2 shows a spectrum taken three days after salt addition, revealing a comparably sharp rising side but considerably broader descending tail. Degradation of either CBPV or its satellite does not take place in the original salt-free suspension stored in a refrigerator for several weeks.

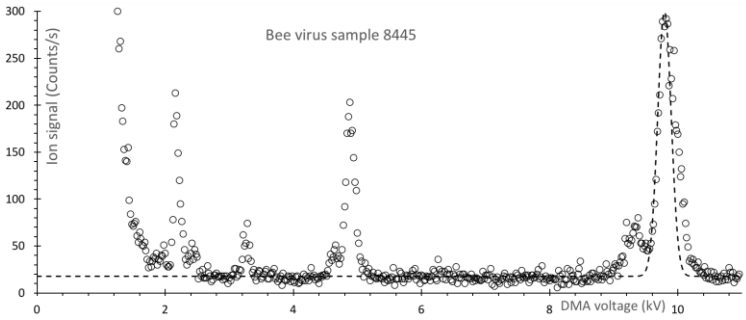

Figure 2: Mobility spectrum for an electrospray of the CBPV solution three days after addition of ammonium acetate, showing the progressive widening of the right tail of the main peak.

Figure 3 shows the evolution of the satellite peak with increasing *Q*. The higher mobility of the satellite now enables much larger *Q* values (up to 303 sL/min) than with the CPB virus, without exceeding the maximal allowed DMA voltage.

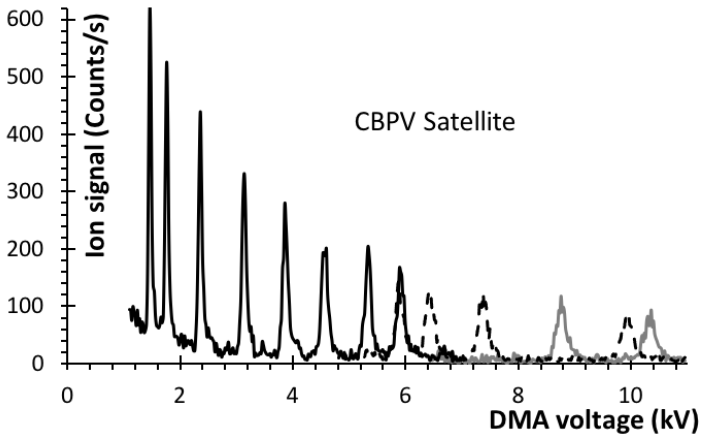

Figure 3: Mobility peaks for the CBPV satellite at flow rates of sheath gas *Q* (sL/min)={43.5; 52; 69; 92;113;135.3; 156; 173.5;189.5; 216; 291.3; 257.1; 303.2}.

The evolution of the resolving power (1/FWHM) associated to the width of each of these peaks is shown in Figure 4. The width has been determined from the data according to several different criteria. *Gaussian all* refers to a fit of the whole peak to a Gaussian curve. This fit reflects best the real FWHM of the measured peak. *Gaussian Left* implies a fitting of the left and top of the peak to a Gaussian, ignoring the right side of the peak potentially contaminated with involatile residues from the solution. *Linear Left* and *Linear All* similarly refer to a fit to either the whole or the left half of the peaks to a triangular peak. That the peaks are approximately triangular, as predicted theoretically in the absence of diffusion (Knutson and Whitby, 1976), can be seen in Figure 3, and in more detail in Figure 5 for a selected group of spectra for the satellite virus. The real peak rounds off the three sharp edges of the triangle at its top and bottom, as a result of either diffusion, or of a finite width of the real particle size distribution (see Figure 2b of Fernandez de la Mora 2017). As a result, the height of the theoretical triangle exceeds slightly that of the experimental peak. This leads to the smaller FWHM of the triangular shape than of the actual peak, explaining why the Gaussian fit data in Figure 4 lie below the linear (triangular) fit data.

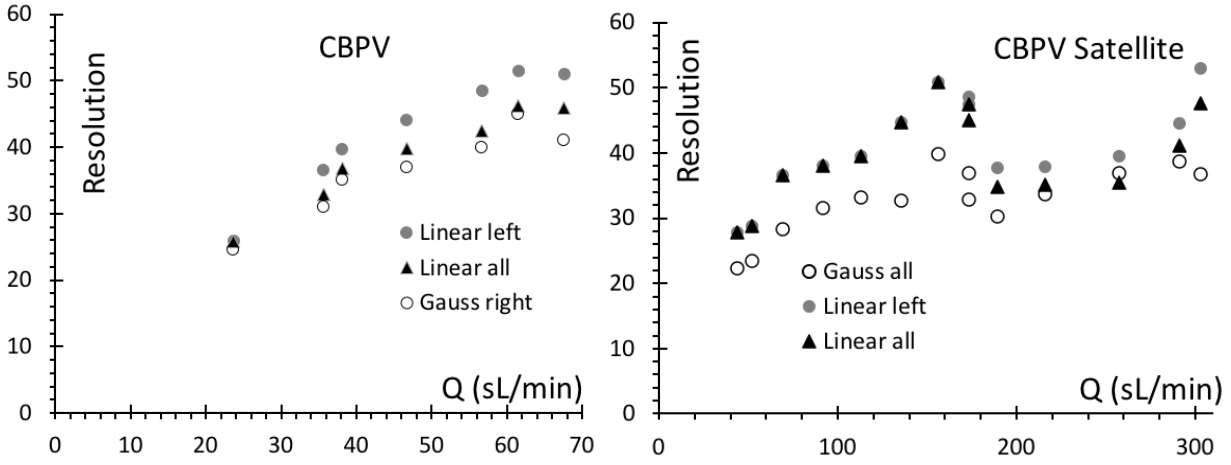

Figure 4: Resolution versus flow rate *Q* of sheath gas for the CBPV (left) and its satellite (right)

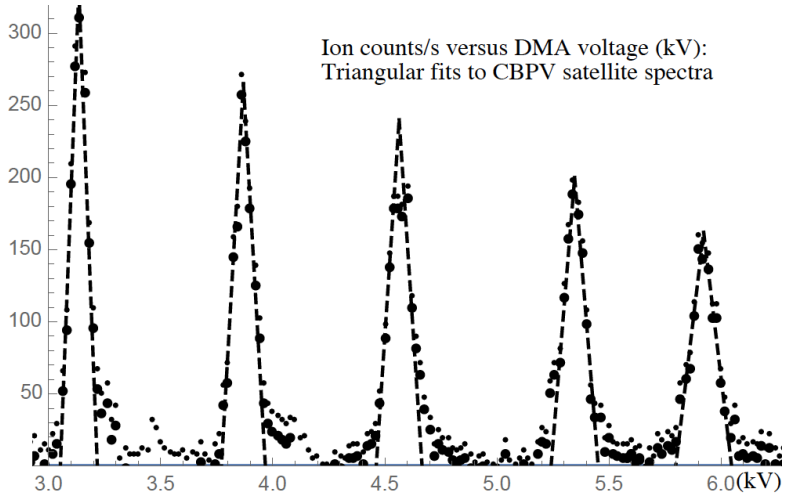

Figure 5: Measured mobility spectra (counts/s versus DMA voltage in kV) for some of the CBPV satellite data of Figure 3. The theoretical triangular shapes are fits to the data.

The high flow data of Figure 4(right) display a sudden loss of resolution taking place abruptly somewhere between 156 and 173.5 sL/min of sheath gas flow. This effect is unrelated to the virus particles, being rather due to the onset of some flow instability in the DMA at a critical flow rate. Other non-idealities of the instrument are evidently broadening the peaks, as the expected FWHM for the triangular peak is expected to equal the ratio *q/Q* between the sheath gas and the aerosol flow, but is in reality larger. Accordingly, the real size distribution of both viral particles studied here is undoubtedly narrower than the FWHM values measured. Therefore, the development of improved DMAs is likely to show that virions electrosprayed into the gas phase may have remarkably narrow size distributions, with FWHM smaller than the 2% measured here in some cases. This spread in mobility is similar to that previously reported for highly charged HBV capsids, and also comparable to the mass variabilities reported for a number of virions by Jarrold and colleagues (Weiss et al. 2019).

We have not calibrated the new DMA accurately enough to provide a precise quantitative value for the mobility diameter of the two particles studied. However, work at BVS based on the known dimensions of TSI's DMA and measured flow rates establishes that the main peak in the same CBPV sample used here (and in many prior measurements) has a diameter of about 37 nm. Based on the measured mobility ratio of 4.5 between the main peak and its satellite (Figure 1 left), the mobility diameter of the satellite would be 16.96 nm. This is pretty close to the BVS measurement for this sample and to prior measurements for this satellite particle. Note however that the satellite rises very close to the large protein background present at low mobilities, so its peak has been previously imperfectly resolved from the rapid rise of the background at decreasing voltages. This problem can still be seen in Figure 1 (left), even though a much better isolation of this peak is facilitated here both by the additional dialysis of the sample (that decreases the background) and by the higher resolving power of our DMA (that concentrates the viral peak into a narrower voltage range).

4. CONCLUSIONS

Combining improvements in the resolving power of our viral DMA with the use of bee viruses widely studied previously by DMA analysis, we have observed viral peak widths as small as 2% in mobility at 17 and 37 nm in diameter. This corresponds approximmately to FWHM as small as

1% in diameter and relative standard size deviation below 0.5%. These exceptionally narrow values are still limited by observed nonidealities in both the DMA and the electrospraying process, suggesting that the viral particles themselves may have substantially narrower intrinsic size distributions than the bounds established here by the imperfect tools presently available.

REFERENCES

Fenn, J. B.; Mann, M.; Meng, C. K.; Wong, S. F.; Whitehouse, C. M. (1989) Electrospray Ionization for Mass Spectrometry of Large Biomolecules, Science, 246, 64−71.

Fernandez de la Mora, J. (2015) High-Resolution Mobility Analysis of Charge-Reduced Electrosprayed Protein Ions, *Anal. Chem*., 87, 3729−3735

Fernandez de la Mora, J., Barrios, C. (2017) A Bipolar electrospray source of singly charged salt clusters of precisely controlled composition, Aerosol Sci. Techn., 51(6) 778-786, 2017

Fernandez de la Mora, J. (2017) Expanded flow rate range of high-resolution nanoDMAs via improved sample flow injection at the aerosol inlet slit, J. Aerosol Sci. 113, 265-275.

Fernandez de la Mora, J. (2018) Mobility analysis of Proteins by charge-reduction in a bipolar Electrospray source, Anal. Chem., 90 (20), 12187–12190

Fernández García, J., Compton, S., Wick, C., Fernandez de la Mora, J. (2019) Virus size analysis by gas phase mobility measurements: Resolution limits. Analytical Chemistry, 91, 20, 12962-12970

Kallinger, P., Weiss, V. U., Lehner, A., Allmaier, G., Szymanski, W. W. (2013) Analysis and handling of bio-nanoparticles and environmental nanoparticles using electrostatic aerosol mobility, *Particuology* 11, 14-19

Kaufman, S. L., Zarrin, F. Dorman, F. (1993) Electrospray apparatus for producing uniform submicrometer droplets, U.S. Patent No. 5, 247,842.

Kaufman, S. L.; Skogen, J. W.; Dorman, F. D.; Zarrin, F.; Lewis, K. C. (1996) Macromolecule Analysis Based on Electrophoretic Mobility in Air: Globular Proteins, *Anal. Chem*., 68,1895-1904

Knutson, E. O., and K. T. Whitby (1975). Aerosol Classification by Electric Mobility: Apparatus Theory and Applications, J. Aerosol Sci. 6:443-451.

Perez-Lorenzo, L. J., Khanna, V.; Meena, T., Fernandez de la Mora, J. (2020) A high resolution DMA covering the 1-67 nm size range, Aerosol Sci & Techn., 54:1, 128-142

Perez-Lorenzo, L. J., Fernandez de la Mora, J. (2021) Improved DMA for high-resolution viral particle studies. To be submitted to Aerosol Science and Techn.

Ribière, M., Olivier, V., Blanchard, P. (2010). Chronic bee paralysis: A disease and a virus like no other? J. Invertebrate Pathology 103, S120–S131

Uetrecht, C., Rose, R. J., van Duijn, E., Lorenzen, K., Heck, A. J. R. (2010) Ion mobility mass spectrometry of proteins and protein assemblies, Chem. Soc. Rev., 39, 1633–1655

Weiss, V.U., Pogan, R., Zoratto, S., Kevin M. Bond, P. Boulanger, M. F. Jarrold, Ni. Lyktey, D. Pahl, N. Puffler, M. Schelhaas, E. Selivanovitch, C. Uetrecht, G. Allmaier (2019) Virus-like particle size and molecular weight/mass determination applying gas-phase electrophoresis (native nES GEMMA)Anal Bioanal Chem. 411: 5951.

Wick, C. H. (2015) Detecting Viruses in Honeybees, Chapter 10 In *Integrated Virus Detection,* CRC Press, , Boca Raton London New York

You, R., Li, M., Guha, S., Mulholland, G. W., Zachariah, M. R., (2014) Bionanoparticles as Candidate Reference Materials for Mobility Analysis of Nanoparticles, Anal. Chem., 86, 6836−6842